

The Pennsylvania State University
The Graduate School
Department of Chemical Engineering

**EFFECTS OF ELECTROLYTE ON THE CATHODE PERFORMANCE OF
MICROBIAL FUEL CELLS AND MICROBIAL ELECTROLYSIS CELLS**

A Thesis in
Chemical Engineering
by
Iman Shahidi Pour Savizi

© 2010 Iman Shahidi Pour Savizi

Submitted in Partial Fulfillment
of the Requirements
for the Degree of

Master of Science

May 2010

The thesis of Iman Shahidi Pour Savizi was reviewed and approved* by the following:

Michael J. Janik
Assistant Professor of Chemical Engineering
Thesis Advisor

Bruce E. Logan
Kappe Professor of Environmental Engineering

Darrell Velegol
Professor of Chemical Engineering

Andrew Zydney
Professor of Chemical Engineering
Head of the Department of Chemical Engineering

*Signatures are on file in the Graduate School

ABSTRACT

Anion adsorption affects electro-catalytic reaction rates by blocking active sites, altering adsorbed species stability, or modifying the electrostatic potential distribution at the interface. Of specific interest are adsorbed anion effects on electrode kinetics at microbial fuel cell and microbial electrolysis cell cathodes, where oxygen reduction reaction (ORR) and hydrogen evolution reaction (HER) occur. These cells operate in buffered solutions containing various anions. Experimental electrode kinetics studies and density functional theory (DFT) are applied to investigate the anion adsorption impact on electrode kinetics. Acetate, dihydrogen and hydrogen phosphate effects are considered on platinum cathodes. DFT predicts the coverage of these anions on the surface as a function of electrochemical potential. The computational results show that acetate and dihydrogen phosphate adsorb at the platinum surface at potentials less than the equilibrium potential of the ORR and greater than the equilibrium potential of the HER. The rate of ORR can therefore be affected due to the adsorption of these anions. Hydrogen phosphate has no effect on ORR and HER because it adsorbs on platinum at potentials greater than the equilibrium potential for these two reactions. Linear sweep voltammetry (LSV) is used to evaluate HER and ORR kinetics in the presence of various anions. Experimental results show that the ORR rate was decreased in the presence of acetate and dihydrogen phosphate. The HER rate was increased in the presence of dihydrogen phosphate due to the “weak acid effect” of this anion. The computational results exclude the adsorption and surface reduction of phosphate anions as a possible mechanism for the “weak acid effect.”

TABLE OF CONTENTS

LIST OF FIGURES	v
LIST OF TABLES	vii
ACKNOWLEDGEMENTS	viii
Chapter 1 Introduction	1
Anion adsorption effect	4
Proton re-generation of phosphate species	8
Electrochemical deprotonation of phosphate species	9
Weak acid reduction:	10
Chapter 2 A First Principles Investigation of Specific Acetate and Phosphate Species	
Adsorption at Pt(111) electrode	12
Computational methods	12
Electronic structure methods	12
Vacuum slab, linear free energy model	13
Applied external electric field	15
Water bilayer-applied external electric field model	16
Double reference method	17
Linear sweep voltammetry simulation	18
Results and discussion	19
Acetate adsorption	19
Effect of surface coverage on acetate adsorption	21
Comparison of computational methods for acetate adsorption	24
Dihydrogen phosphate adsorption	27
Hydrogen phosphate adsorption	31
Chapter 3 LSV of oxygen reduction and hydrogen evolution reaction on platinum surface in presence of anions	36
Experimental methods	36
LSV of the oxygen reduction reaction	37
LSV of the hydrogen evolution reaction	38
Chapter 4 Conclusions	40
References	41

LIST OF FIGURES

Figure 1-1: Schematic diagram of microbial fuel cell ($\text{HCO}_3^- = 5 \text{ mM}$, $\text{CH}_3\text{COO}^- = 16.9 \text{ mM}$, $\text{pO}_2 = 0.2$, $\text{pH} = 7$).	1
Figure 1-2: Schematic diagram of microbial electrolysis cell ($\text{HCO}_3^- = 5 \text{ mM}$, $\text{CH}_3\text{COO}^- = 16.9 \text{ mM}$, $\text{pO}_2 = 0.2$, $\text{pH} = 7$).	2
Figure 1-3: Schematic of the electrochemical deprotonation of phosphate ions.	10
Figure 2-1: Preferred adsorption configuration of acetate over Pt(111) (a) vacuum slab model top view (b) vacuum slab model side view (c) water bilayer-external electric field model (d) double reference method	20
Figure 2-2: Adsorption free energy of acetate to the Pt(111) surface for different surface coverages using the vacuum slab model. ($T=298 \text{ K}$, $[\text{CH}_3\text{COO}^-_{\text{aq}}] = 0.2 \text{ M}$, $U=0$ (SHE))	21
Figure 2-3: Simulated linear sweep voltammetry of acetate adsorption at Pt(111) and the amount of acetate coverage using vacuum slab model with surface coverage effect (solid lines) and without surface coverage effect (dashed lines). ($T=298 \text{ K}$, $[\text{CH}_3\text{COO}^-_{\text{aq}}] = 0.2 \text{ M}$, $v = 30 \text{ mV s}^{-1}$).....	22
Figure 2-4: Adsorption free energy of acetate on Pt(111) at different potential for different models. ($T=298 \text{ K}$, $[\text{CH}_3\text{COO}^-_{\text{aq}}] = 0.2 \text{ M}$).	25
Figure 2-5: Simulated linear sweep voltammetry of acetate adsorption at Pt(111) for different models. ($T=298 \text{ K}$, $[\text{CH}_3\text{COO}^-_{\text{aq}}] = 0.2 \text{ M}$, $v = 30 \text{ mV s}^{-1}$).....	26
Figure 2-6: Simulated linear sweep voltammetry of acetate adsorption at Pt(111) using double reference method. ($T=298 \text{ K}$, $[\text{CH}_3\text{COO}^-_{\text{aq}}] = 0.01 \text{ M}$, $v = 30 \text{ mV s}^{-1}$).	27
Figure 2-7: Preferred adsorption configuration of dihydrogen phosphate over Pt(111) (a) vacuum slab model top view (b) vacuum slab model side view (c) double reference method.....	29
Figure 2-8: Adsorption free energy of dihydrogen phosphate on Pt(111) at different potential for vacuum slab model (dashed line) and the double reference method (solid line). ($T=298 \text{ K}$, $[\text{H}_2\text{PO}_4^-_{\text{aq}}] = 0.01 \text{ M}$).....	29
Figure 2-9: Simulated linear sweep voltammetry of dihydrogen phosphate adsorption at Pt(111) for vacuum slab model (dashed line) and the double reference method (solid line). ($T=298 \text{ K}$, $[\text{H}_2\text{PO}_4^-_{\text{aq}}] = 0.001 \text{ M}$, $v = 50 \text{ mV s}^{-1}$).....	30
Figure 2-10: Preferred adsorption configuration of hydrogen phosphate over Pt(111) (a) vacuum slab model top view (b) vacuum slab model side view (c) double reference method.....	32

Figure 2-11: Adsorption free energy of hydrogen phosphate on Pt(111) at different potential for vacuum slab model (dashed line) and the double reference method (solid line). (T=298 K, $[\text{HPO}_4^-]_{\text{aq}} = 0.01 \text{ M}$)	33
Figure 2-12: Simulated linear sweep voltammetry of hydrogen phosphate adsorption at Pt(111) for vacuum slab model (dashed line) and the double reference method (solid line). (T=298 K, $[\text{H}_2\text{PO}_4^-]_{\text{aq}} = 0.01 \text{ M}$, $v = 1 \text{ mV s}^{-1}$)	34
Figure 3-1: Experimental setup to record the LSV data.	37
Figure 3-2: Linear sweep Voltammograms for ORR at the platinum disc. All LSV recorded at $v = 5 \text{ mVs}^{-1}$	38
Figure 3-3: Linear sweep Voltammograms for HER at the platinum disc. All LSV recorded at $v = 5 \text{ mVs}^{-1}$	39

LIST OF TABLES

Table 2-1: Features of the adsorption peak and free energy of adsorption predicted by different methods.	26
---	----

ACKNOWLEDGEMENTS

I would like to give my thanks and appreciation to the following people:

I would like to thank Dr. Michael J. Janik my thesis advisor for all of his help, support and encouragement through this study.

I would like to thank Dr. Bruce E. Logan for all of his help and financial support through this study.

I would also like to thank my wife, Sepideh Mohamadzadeh, who has always helped and supported me.

I would also like to thank my family especially my father and mother.

I would also like to thank my best friend, Gholamreza Rostamikia, who has always helped me during this study.

Chapter 1

Introduction

One of the main challenges of scientists today is finding new sources of energy. The main source of energy we use is fossil fuels, particularly oil and gas. Fossil fuels cannot support our energy demand beyond the next 100 years, and also using these fuels is proposed as the main cause of global climate change. Thus, renewable and clean source for energy production is necessary for our world. Microbial Fuel Cells (MFCs) and Microbial Electrolysis Cells (MECs) may contribute to reducing our reliance on fossil fuels for energy production [1-3].

A MFC is a device that converts the chemical energy of organic compounds to electricity by using microbes as the catalyst. A schematic diagram of a MFC is demonstrated in Fig. 1-1.

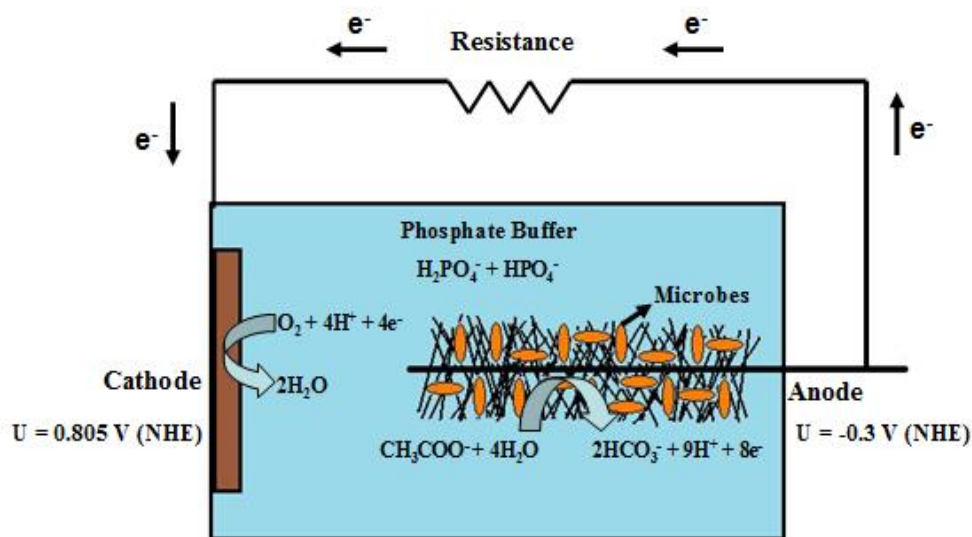


Figure 1-1 Schematic diagram of microbial fuel cell ($\text{HCO}_3^- = 5 \text{ mM}$, $\text{CH}_3\text{COO}^- = 16.9 \text{ mM}$, $p\text{O}_2 = 0.2$, $\text{pH} = 7$).

At the anode, microbes oxidize organic chemical matter to carbon dioxide, electrons and protons. Electrons through the external wire transfer to the cathode, and the protons migrate

through the solution to the cathodic chamber. Oxygen reacts with protons and electrons on the cathode and it is reduced to water.

The MEC is a modified form of MFC which is shown in Fig. 1-2. Oxygen is not provided to the cathode side as in the MFC, and a potential is applied to produce hydrogen gas in cathode chamber. MEC is able to convert biomass into hydrogen gas through the electro-hydrogenesis process. In this process, microbes in the anode chamber consume the organic compounds and produce protons, electrons and carbon dioxide. Protons migrate in the solution to the cathode, and by adding a voltage boost to the inherent oxidation voltage, the hydrogen evolution reaction (HER) is favorable at the cathode.

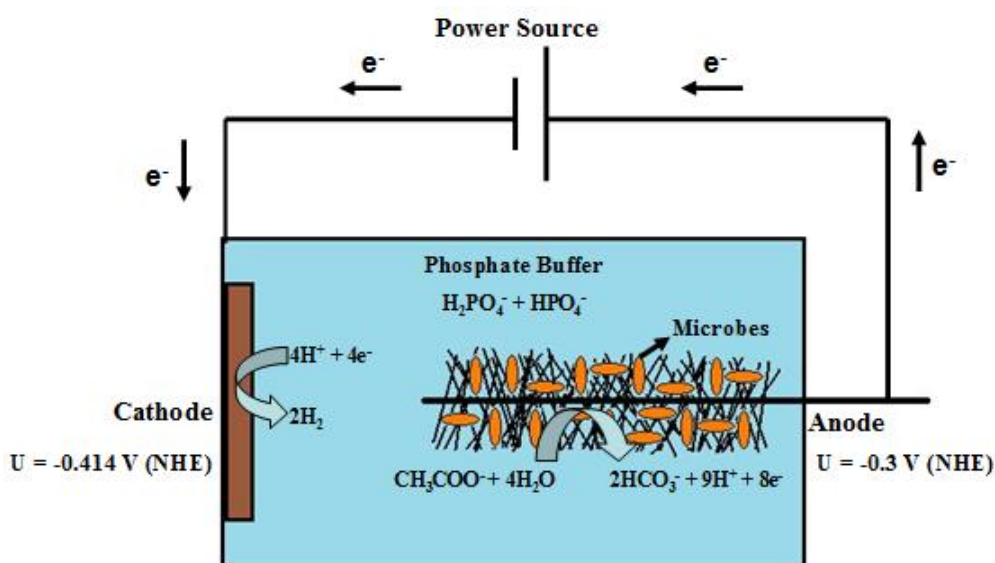


Figure 1-2 Schematic diagram of microbial electrolysis cell ($\text{HCO}_3^- = 5 \text{ mM}$, $\text{CH}_3\text{COO}^- = 16.9 \text{ mM}$, $p\text{O}_2 = 0.2$, $\text{pH} = 7$).

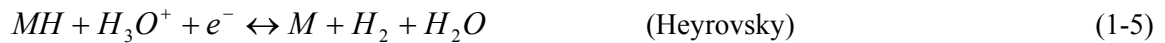
There have been a lot of efforts to improve the efficiency of MFCs and MECs. Single chamber MFCs and MECs have been used to reduce the internal resistance by eliminating the membrane from the system [4]. Using anodes with high surface area for microbial colonization can avoid rate limitations due to the anode reaction [2]. Given a device construction in which

electrolyte and anode resistance are minimized, ORR and HER occurring at the cathode may limit the overall device performance. Therefore, greater understanding of the processes occurring in these cathode reactions is essential for rational improvement in cathode, and therefore MFC and MEC device performance.

The oxygen reduction reaction happens in many fuel cells. Hence, this reaction has been investigated in many electrolytes and on a lot of materials. Platinum is a good catalyst for ORR because it has a high activity in acidic media for this reaction. The Damjanovic mechanism for ORR in acidic media, which is widely accepted, is [5]:



The hydrogen evolution reaction has been studied widely due to the different applications of this electrochemical reaction such as water electrolysis to produce hydrogen gas. It is widely accepted that the initial reaction in the HER is adsorption of a hydrogen ion at the metal surface. This first step is called the Volmer reaction which is followed by Heyrovsky or Tafel reactions. The Tafel reaction is not an electrochemical reaction, so the rate of this reaction is not dependent on potential of the metal surface.



It is usually presumed that rate determining reaction in HER mechanism is one of the above forward reactions.

The cathode and the anode in MFCs and MECs work at near neutral pH conditions, because microbes live at the neutral pH. In laboratory studies, phosphate buffer is usually used for keeping the pH near 7. In membrane-less MFCs and MECs, the cathode encounters buffer anions as well as anionic species derived from the fuel. These anions may alter HER and ORR kinetics compared to those under acidic conditions. In this work, we examine the effects of anions on the HER and ORR cathodic reactions.

Anions can affect the ORR and HER rate by different ways. They can adsorb at the cathode and block the active sites, or affect double-layer structure, or alter the solution conductivity. We investigate two possible theories about the anions effect on the rate of HER and ORR: 1- Anion adsorption: in this theory anion can adsorb at the cathode and block the active sites, and reduce the rate of ORR and HER. 2- Proton re-generation of phosphate species: phosphate species can undergo solution phase protonation/ deprotonation reactions and alter the concentration of the reactant protons available for reactions. In below each of these theories are described.

Anion adsorption effect

Anion adsorption can affect electro-catalytic reaction rates by blocking active sites, altering adsorbed species stability, changing electrical double layer (EDL) structure, or modifying the electrostatic potential distribution at the interface[6-8]. Specific adsorption of anions, including acetate, dihydrogen and hydrogen phosphate, may affect electrode kinetics at microbial fuel cells (MFCs) and microbial electrolysis cells (MECs) cathodes where the oxygen reduction reaction (ORR) [1] and the hydrogen evolution reaction (HER) occur [2]. Adsorption of phosphate species on platinum electrodes can increase their acid strength by altering the deprotonation equilibria [9-11]. This process leads to increase the proton concentration on the

electrode surface which is favorable in MECs. Adsorbed phosphate species can reduce the rate of ORR by blocking the active sites in phosphoric acid fuel cells (PAFCs). Acetate is an intermediate in the electrochemical oxidation of ethanol in direct ethanol fuel cells (DEFCs) and its adsorption equilibrium affects selectivity to complete oxidation. Voltammetry may be used to evaluate the thermodynamics and kinetics of ion adsorption, and surface sensitive spectroscopic techniques such as surface enhanced Raman spectroscopy (SERS) or attenuated total reflection infrared (ATR-IR) spectroscopy can be used to probe the molecular structure of adsorbed species. However, these methods are limited in their ability to isolate the ion adsorption process, and characterize directly the metal adsorbate interaction at the electrode-electrolyte interface. Density functional theory (DFT) methods are widely applied to investigate adsorption on metal catalysts, and herein we evaluate a series of approaches to investigate the thermodynamics of anion adsorption at metal electrode surfaces. We consider acetate and phosphate species adsorption to the Pt(111) surface and apply a series of approaches to take solvation and interfacial electric field into account. These DFT methods are used to predict the coverage of specifically adsorbed anions as a function of potential and to simulate a linear sweep voltammogram.

Electrodes of membrane-less MFCs or MECs operate in buffered solutions containing various anions [4, 12]. Phosphate buffer, containing dihydrogen and hydrogen phosphate, is typically used in the laboratory to maintain the pH near the neutral condition necessary for growing the microbes [12]. Acetate is a typical substrate used for fuel in the MFCs/MECs. The rates of the ORR and HER on the cathode side are known to be affected by the identity and concentration of buffer solutions [13, 14]. A contributions process to alter the rates of these reactions may be site blocking by specific adsorption of anions. Cathode electrodes in MFC and MEC are often made of platinum. Determination of the potential dependent coverage of anions, for a given concentration, will aid understanding of the ORR and HER in these cells.

Phosphate and acetate adsorption processes are relative to the PAFCs and DEFCs. PAFCs use phosphoric acid liquid electrolyte, and phosphate adsorption to platinum/carbon electrodes can inhibit the ORR [6, 7]. A DEFC produces energy by oxidizing ethanol to water and dioxide carbon. Adsorbed acetate is suggested as one of the intermediates in the mechanism of the electro-oxidation of ethanol on platinum [15], and the relative preference to desorb versus further oxidize will influence the selectivity to acetic acid production versus complete oxidation.

The first voltammetric study of phosphate adsorption over platinum was conducted by Clavilier and co-workers [16, 17]. They observed a peak in the cyclic voltammetry (CV) and suggested that peak is related to phosphate species adsorption. Later, Taguchi and co-workers reported cyclic voltammogram characteristics for adsorption of anions from phosphate and other solutions [18]. They found that the position of the phosphate adsorption peak was dependent on pH. Fukuda and Aramata studied the kinetic of adsorption/desorption of phosphate anions on Pt(111) in acidic solutions by using a potential step method [19]. They observed an adsorption peak in a 0.3 M solution of KH_2PO_4 of pH 4.3 which begins at -0.4 V (SHE) and ends at 0 V (SHE). They employed the Langmuir and Elovich isotherms to analyze the adsorption processes. At low coverage, adsorbed anions have no interactions with each other and adsorption process can be predicted by Langmuir isotherm, while at high coverage, adsorption occurs with repulsive interactions between adsorbed phosphate species. The thermodynamic features of phosphate adsorption at Pt(111) electrode was studied by Mostany and co-workers [20] in perchloric acid. They reported the phosphate adsorption peak in a solution of 0.1 M HClO_4 + 0.01 M NaH_2PO_4 and some other phosphate concentrations which starts around 0.3 V (SHE) and ends around 0.7 V (SHE). The first spectroscopic experiments of phosphate anions on a platinum electrode in perchloric acid were developed by Habib and Bockris [21]. Ye et al. used the in situ FTIR spectroscopy to study the adsorption of phosphate species on single crystal platinum in a wide pH range [22] which can help us to find the orientation of adsorbed phosphate species on surface.

Bidoia monitored the adsorption of dihydrogen phosphate on platinum surface by probe-beam deflection (PDB) which is an in situ and non-spectroscopic technique [23]. He concluded that Langmuir isotherm is appropriate to model the dihydrogen phosphate adsorption on platinum surface.

The adsorption of acetate in perchloric solution was observed by Orts and co-workers [24]. They reported that acetate adsorption occurred in the same potential region as the adsorption of sulfate on Pt(111) which was illustrated using CO displacement method. Fukuda and Aramata investigated the kinetics and mechanism of adsorption/desorption of acetate on Pt(111) electrode in acidic media by using cyclic voltammetry and potential step method [25]. They observed the adsorption peak of acetate in 0.2 M solution of $\text{CH}_3\text{COOH} + \text{CH}_3\text{COOK}$ of different pH, which acetate begins to adsorb at -0.5 V (SHE) and stops adsorbing at -0.15 V (SHE). They reported that Langmuir isotherm is a good model for acetate adsorption at low coverage, but at higher coverage, adsorption with repulsive forces took place. In situ FTIR spectroscopy have been employed to specify the configuration of adsorbed acetate on platinum electrode surface [26].

Although experiments have provided considerable information about the thermodynamics, kinetics, and structure of anion adsorption, atomistic detail of the adsorbed structure and the importance of solvation and field affects are limited. Characterization of adsorption at the electrode-electrolyte is a challenging problem because the properties and behavior of interfacial water molecules are different from the bulk molecules [27-30]. Electronic structure technique can provide detailed characterization of the bonding interaction of species to metal surfaces. Density functional theory (DFT) is widely used to investigate adsorption and reaction at metal surfaces, and approaches to represent electrochemical processes are available. Application of an external electric field within a metal/vacuum interface model has been used to investigate the impact of potential alternation on the adsorption process [31, 32]. Although this approach can model the effects of EDL, it does not consider the adsorbate-solvent, solvent-

solvent and solvent-metal interactions at the electrode-electrolyte interface. In another approach, Nørskov and co-workers model the electrochemical environment by changing the number of electrons and protons in a water bilayer on a Pt(111) surface [33, 34]. Jinnouchi and Anderson used the modified Poisson-Boltzmann theory and DFT to simulate the solute-solvent interaction to integrate a continuum approach to solvation and double layer effects with a DFT system [35].

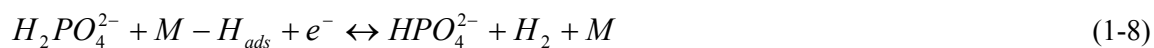
In this study, a series of DFT approaches is applied to investigate anion adsorption at the electrode interface. In the simplest approach, analogous to the method used by Nørskov et al. [36] and Anderson and Kang [37], anion adsorption is taken to occur with the transfer of an electron, and the electron energy changes linearly with potential while the adsorbate energy is potential independent. The impact of an electric field during the adsorption process is tested in an applied external electric field model. Intermolecular interactions with interfacial solvent molecules within a charged double layer model are simulated with the double reference method developed by Neurock and co-workers [38, 39]. The results of these DFT methods are used to simulate the LSV and to predict the surface coverage of adsorbate as a function of surface potential. The simulated voltammetric experiment data is compared with experimental data from the literature. The effect of surface coverage on the adsorption process will also be discussed.

Proton re-generation of phosphate species

It was observed by some researchers that the presence of weak acid phosphate species in the solution decreased the HER over-potential and increased the HER rate [3, 14]. There are two possible ways that phosphate species generate protons in the solution: 1- Electrochemical deprotonation, 2- Weak acid reduction. We will try to figure out by which method phosphate species produce protons for HER. In the following, these two methods are described.

Electrochemical deprotonation of phosphate species

The unexpected increase in HER rate in phosphate solution may be caused by the electrochemical deprotonation of phosphate ions on platinum surface [9, 11, 40, 41]. O'Neil and co-workers [41], and then Takehara and co-workers [11] proposed that at low pH, $H_2PO_4^-$ interacts with an electron to create an adsorbed hydrogen atom, which may also react with another $H_2PO_4^-$ ion to produce a hydrogen molecule:



where M is the metal. At higher pH, both $H_2PO_4^-$ and HPO_4^{2-} may interact with the surface of electrode and deprotonate:



The schematic of the electrochemical deprotonation of phosphate ions is illustrated in Fig. 1-3. The first step of the reaction 1 and 3 is adsorption of $H_2PO_4^-$ and HPO_4^{2-} on the metal surface [40, 41]. Hence, to evaluate whether this is a possible mechanism of promotion of the HER by weak acids, we can examine at what potential range these anions can adsorb to the metal surface. We would expect that adsorption produces a significant coverage of $H_2PO_4^-$ and HPO_4^{2-} during the HER if this mechanism is dominant. Furthermore, were this the case, then the rational choice of cathode electro-catalysis for this system would need to consider the activity for surface reactions involving the phosphate species, and could therefore lead to optimal materials that differ from the non-buffered, acidic conditions. In the next chapter, adsorption of these ions on the platinum surface will be investigated.

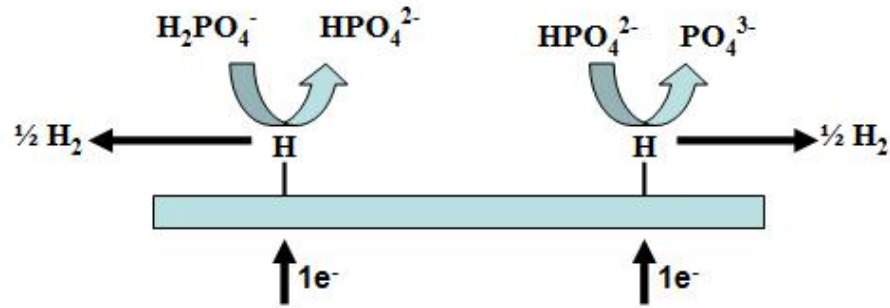


Figure 1-3 Schematic of the electrochemical deprotonation of phosphate ions.

Weak acid reduction:

Weak acid reduction is another mechanism to interpret the increase in HER rate in phosphate solution. This mechanism is of the chemical-electrochemical type, where the electrochemical reduction of protons occurs after the dissociation of the weak acid [3, 42]:



The weak acid presence would therefore accelerate the overall reaction by “re-supplying” protons in the depletion region near the electrode. Daniel and co-workers [42] proposed an equation to calculate the limiting current gained on platinum microelectrodes:

$$I_L = 4F \times r(D_{H^+}[H^+] + D_{HA}[HA]) \quad (1-13)$$

where I_L is the limiting current, F is the Faraday constant, r is electrode radius and D is the diffusion coefficient. Equation 1-13 shows that the limiting current depends on the concentration of both proton ($[H^+]$) and un-dissociated acid ($[HA]$). This equation has been used to test whether the HER mechanism in phosphate solution matches with above mechanism (equations 1-11 and 1-12). Were the main role of the weak acid to regenerate protons depleted from the

solution region near the electrode, then the surface reduction mechanism would not differ from acidic conditions and therefore the electro-catalysts showing the greatest activity for HER in the weak acid solution would not expect to differ.

Chapter 2

A First Principles Investigation of Specific Acetate and Phosphate Species Adsorption at Pt(111) electrode

Anion adsorption can affect the electro-catalytic reaction rates by blocking active sites and reducing the electrode surface area. In this chapter, density functional theory (DFT) is applied to investigate the anion adsorption impact on electrode kinetics. Adsorption of acetate, dihydrogen and hydrogen phosphate are investigated on the Pt(111) surface. DFT methods are used to predict the coverage of these anions on the surface as a function of electrochemical potential. The adsorption free energy of each anion on Pt(111) is calculated, and using these results, we simulated the linear sweep voltammogram related to anion adsorption. Effects of surface coverage and methodological choices in model construction were considered for their impact on the simulated voltammogram. The double reference method produces simulated data in best agreement with experimental voltammograms.

Computational methods

Electronic structure methods

All calculations were executed using the ab initio total-energy and molecular-dynamics Vienna ab initio simulation program (VASP) developed at the Institute for Material Physics at the University of Vienna [43-45]. Exchange and correlation energies were calculated using the Perdew-Wang (PW91) form of the generalized gradient approximation (GGA) [46]. The projected augmented wave (PAW) method [47] and 450 eV cut of energy for the plane-wave basis set were used in representing core and valence electron interactions. Gamma pack mesh was used to carry out Brillouin-zone sampling. The forces on all atoms were minimized to less than

0.05 eV Å⁻¹ in the structural optimization procedure. All the adsorption calculations were carried out spin-restricted, and testing on a subset of structures indicated no difference in the energy of system when spin polarized. Zero point vibrational energy (ZPVE) corrections were calculated using the harmonic vibrational modes of surface adsorbates. The platinum experimental lattice constant (3.92 Å) was employed for all of the calculations.

The following four sections detail the DFT model constructions and calculations of the potential dependent Gibbs free energy of adsorption using each. Section fifth provides the approach for simulating the LSV using the calculated adsorption free energy.

Vacuum slab, linear free energy model

A vacuum slab model is the simplest approach to representing the electrode-electrolyte interface. This model quantifies the interaction energy between the adsorbate and metal surface while neglects the interaction between adsorbate-solvent and the interfacial electric field. The energy of the electron transferred upon anion adsorption is linear with electrode potential, and is the only potential dependent term in the adsorption free energy. Because of the simplicity, this method has been used widely by other researchers. Nørskov et al. [36] used similar method to model water oxidation and oxygen reduction.

A five layers metal slab with the top two layers relaxed and the three bottom layers fixed to platinum fcc lattice positions was used to model the Pt(111) surface in all model constructions. Different surface coverages were examined for acetate adsorption using 1x2, $\sqrt{3} \times \sqrt{3}$, 2x2, 3x3, 4x4 and each has the kpoints of 9x9x1, 7x7x1, 7x7x1, 3x3x1, 3x3x1 respectively. A vacuum space equal to eight platinum layers was included between periodic surface slabs. All possible orientations of the anions including high symmetry atop, bridge, hcp and fcc hollow sites were examined and the orientation with lowest energy chose for calculations of adsorption energy.

Dipole interactions between slabs repeated along the surface normal were corrected for within the electron self consistent field cycles (VASP keyword LDIPOL). The adsorption reaction of anions (A_{aq}^-) on the metal surface (*) to form adsorbed species (A^*) and release an electron is written as:



In real conditions when an anion from bulk adsorbs on a metal surface, a water molecule desorbs to bulk (water displacement effect). The free energy difference of anion adsorption (ΔG_{ads}) is calculated as:

$$\Delta G_{ads}(U) = G_{A^*} + G_{H_2O_{aq}} - eU - G_{A_{aq}^-} - G_{H_2O^*} \quad (2-2)$$

where U is the absolute potential (relative to vacuum electrode) of metal, $-e$ is the charge of an electron, $G_{H_2O^*}$ is the free energy of adsorbed water molecule on metal surface, and $G_{H_2O_{aq}}$ is the Gibbs free energy of water molecule in solution and is equal to -14.353 eV [48]. Results are demonstrated with the potential relative to a standard hydrogen electrode using the equation [48]:

$$U_{SHE} = U - 4.6 \quad (2-3)$$

where U_{SHE} is potential relative to a standard hydrogen electrode. The free energy of adsorbed species (including water molecule) (G_{A^*}) and anions in aqueous phase ($G_{A_{aq}^-}$) were determined using:

$$G_{A^*} = E_{DFT} - S_{vib}T + ZPVE \quad (2-4)$$

$$G_{A_{aq}^-} = G_{A_{gas}^-} + \Delta G_{Hydration}^0 + RT \times \ln[A_{aq}^-] \quad (2-5)$$

where E_{DFT} is the electrical energy of adsorbate/metal that was calculated by VASP program, T is temperature on the Kelvin scale, S_{vib} is vibrational entropy at 298.15 K, $G_{A_{gas}^-}$ is given below.

$\Delta G_{Hydration}^0$ is the standard hydration free energy of anion, and $[A_{aq}^-]$ is the anion concentration in solution. The standard hydration energies used here for acetate, dihydrogen phosphate and hydrogen phosphate are $-80 \text{ kcal mol}^{-1}$ [49], $-76 \text{ kcal mol}^{-1}$ and $-299 \text{ kcal mol}^{-1}$ [50] respectively. The free energy of anions in gas phase ($G_{A_{gas}^-}$) was calculated by adding *ZPVE* and entropic terms including translational, vibrational and rotational entropy to the electronic energy of the isolated anion:

$$G_{A_{gas}^-} = E_{DFT} + ZPVE - (S_{trans} + S_{vib} + S_{rot})T \quad (2-6)$$

Applied external electric field

The influence of the external electric field on adsorption of anions on Pt(111) surface was investigated through this model. Construction of this model is equivalent to the model presented in section 2.2 with exceptions of applying an external field (VASP keyword EFIELD), and the only surface coverage used for this model is 3x3. External electric fields including $F = -0.5, -0.25, 0, 0.25$ to 0.5 V \AA^{-1} were applied along the platinum surface normal. The bare metal and adsorbate/metal systems were re-optimized at each field and their free energies are written as:

$$G_{A^*}(F) = E_{DFT,A^*}(F) - S_{vib}T + ZPVE \quad (2-7)$$

$$G_*(F) = E_{DFT,*}(F) \quad (2-8)$$

where $E_{DFT,A^*}(F)$ and $E_{DFT,*}(F)$ are the electrical energy of adsorbate/metal and bare metal, respectively, at a particular electric field. The electrode potential is related to electric field with the following equation:

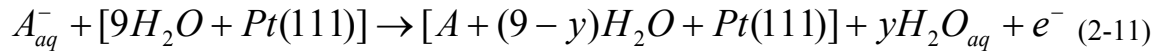
$$U = F \times d \quad (2-9)$$

where U is the electrode potential, F is the external electric field and d is distance between the electrode surface and the counter charge which is assumed to be 3 Å in this paper. Substituting the equation 2-9 in equations 2-7 and 2-8 the free energy difference of anion adsorption ($\Delta G_{ads}(U)$) at specific potential is calculated as:

$$\Delta G_{ads}(U) = G_{A^*}(U) + G_{H_2O_{aq}} - eU - G_{A_{aq}^-} - G_{H_2O^*}(U) \quad (2-10)$$

Water bilayer-applied external electric field model

Construction of this model is same as the model presented in section 2.3 but includes a solvation water layer in cell. An ice-like structure includes nine water molecules used to model the water bilayer on the Pt(111) surface. The formation of a water bilayer has been proved by theory and experiments [29, 30, 51]. Adsorbing of acetate to the surface caused one adsorbed water molecule desorbs to the bulk (water displacement effect). Phosphate adsorption made us to remove two water molecules from the unit cell, one from adsorbed water molecules layer (water displacement effect) and the other one from the upper layer (limitation in z direction). Adsorption reaction is written as:



where [] shows the components in the unit cell. The free adsorption energy is determined as follows:

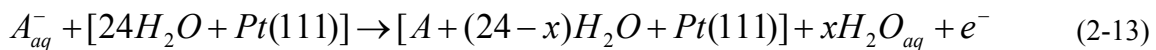
$$\Delta G_{ads}(U) = G_{[A+Pt+(9-y)H_2O]}(U) - yG_{H_2O_{aq}} - eU - G_{A_{aq}^-} - G_{[Pt+9H_2O]}(U) \quad (2-12)$$

The free energy for $[9H_2O + Pt(111)]$ and $[A + (9 - y)H_2O + Pt(111)]$ systems are both field dependent.

Double reference method

The double reference model developed by Neurock and co-workers [38, 39], includes explicit water molecules in the system and varies the electrode charge and counter charge by changing the number of electrons. A 3x3 surface cell was used to model the Pt(111) surface. Twenty four water molecules with an ice-like structure is considered between the periodic slabs to model the water bilayer near the platinum surface. The water density is assumed to be 1 g/cm³, is close to the density of water at ambient conditions, by setting the lattice vector along the surface normal. Two reference potentials are used to calculate the surface potential. The first reference is determined by inserting a vacuum region in the middle of the water molecules and calculating the work function of the neutral system. The second reference is the potential at the center of the water region which is assumed not depend on the charge of the surface.

For calculating the anion adsorption free energy, the ice-like $24H_2O + Pt(111)$ system is optimized and then two (phosphate species adsorption) or three (acetate adsorption) water molecules from the optimized structure are replaced at the surface by adsorbate. Adsorption of acetate on surface made us to replace one molecule from the water layer on the surface (water displacement effect) and two from upper water layers (limitation in z direction). Phosphate species had less limitation in z direction so one molecule from the adsorbed water molecules layer (water displacement effect) and one water molecule from upper layers were replaced. The potential of the electrode is changed by increasing or decreasing the electrons of the system. The system charges used were $ne = -1, -0.5, 0, 0.5$ to 1. A total energy independent of the number of the electrons is calculated as described by Taylor et al. [38]. A quadratic function is fit to the discrete data points to give a potential dependent energy for $24H_2O + Pt(111)$ and $A + (24 - x)H_2O + Pt(111)$ systems, and corrections for *ZPVE* and vibrational entropy of adsorbates is included. The adsorption reaction is represented as:



The free energy difference of the above equation is determined as:

$$\Delta G_{ads}(U) = G_{[A+(24-x)H_2O+Pt(111)]}(U) - xG_{H_2O_{aq}} - eU - G_{A_{aq}^-} - G_{[24H_2O+Pt(111)]}(U) \quad (2-14)$$

Linear sweep voltammetry simulation

Linear sweep voltammetry (LSV) is an electrochemical method that measures the current as a function of potential as the potential is linearly varied with time. If anion adsorption is the only electron transfer process that occurs, then the sweep may be started at a potential at which no anions are adsorbed and swept positive to observe an increase in current as adsorption with electron transfer occurs followed by a decrease as the surface saturated. The potential dependent current may reflect the rate of transport of anions to the surface as well as electron transfer kinetics. However, if these processes are rapid relative to the potential scan rate, then the potential dependent current simply reflects the shifting adsorption equilibrium as the potential is increased.

For simulating the LSV, the adsorption of anions is assumed to maintain equilibrium as the potential is varied. The potential dependent adsorption equilibrium constant is:



$$K(U, \theta) = \exp\left(\frac{-\Delta G_{ads}(U, \theta)}{RT}\right) = \frac{\theta}{(1-\theta)[A^-]} \quad (2-16)$$

where K is the equilibrium constant, θ is the surface coverage A , and the $[A^-]$ is the concentration of the anion in the bulk phase. The adsorption free energy difference as a function of electrode potential can be given by any of the methods described in previous sections. The relation between potential and the scan rate is:

$$U = \nu \times t \quad (2-17)$$

Inserting equation 2-17 into equation 2-16 and solving for θ gives the surface coverage as a function of time. The current density can be calculated as follows:

$$j = \frac{d\theta}{dt} \times \frac{n \times e}{A} \quad (2-18)$$

where j is the current density, n is the maximum number of anions can adsorb per each cell, e is the charge of the electron and A is the surface area for each cell. For example, if an adsorbed anion occupies 3 platinum atoms then for the 3x3 surface n equals to 3 and cell has a surface area of $5.98 \times 10^{-15} \text{ cm}^2$.

Results and discussion

Specific adsorption of acetate, dihydrogen phosphate and hydrogen phosphate over the platinum electrode is studied using density functional theory (DFT), and the linear sweep voltammetry (LSV) of each anion is simulated. Adsorption of acetate at Pt(111) is investigated in first following section. The effect of surface coverage on adsorption free energy is examined in second following section and in third following section; different computational methods are compared with each other. The adsorption of dihydrogen phosphate and hydrogen phosphate on the Pt(111) surface are investigated in fourth and fifth following sections respectively.

Acetate adsorption

The optimal adsorption of acetate to Pt(111) occurs with the C-C bond perpendicular to the surface plane and two O atoms on atop sites (Figs. 1a, b). Rodes and co-workers reported the same adsorption configuration based on FTIR results [26]. The 3x3 vacuum slab surface was

used to confirm this orientation as giving the minimum free energy of adsorption, and this orientation was used as the starting structure for further calculations. Though interval bond distances (including Pt-O) varied with surface cell size, electric field presence, and solvent inclusion, this general adsorption configuration was maintained following structural optimization in all cases (Figs. 2-1c,d).

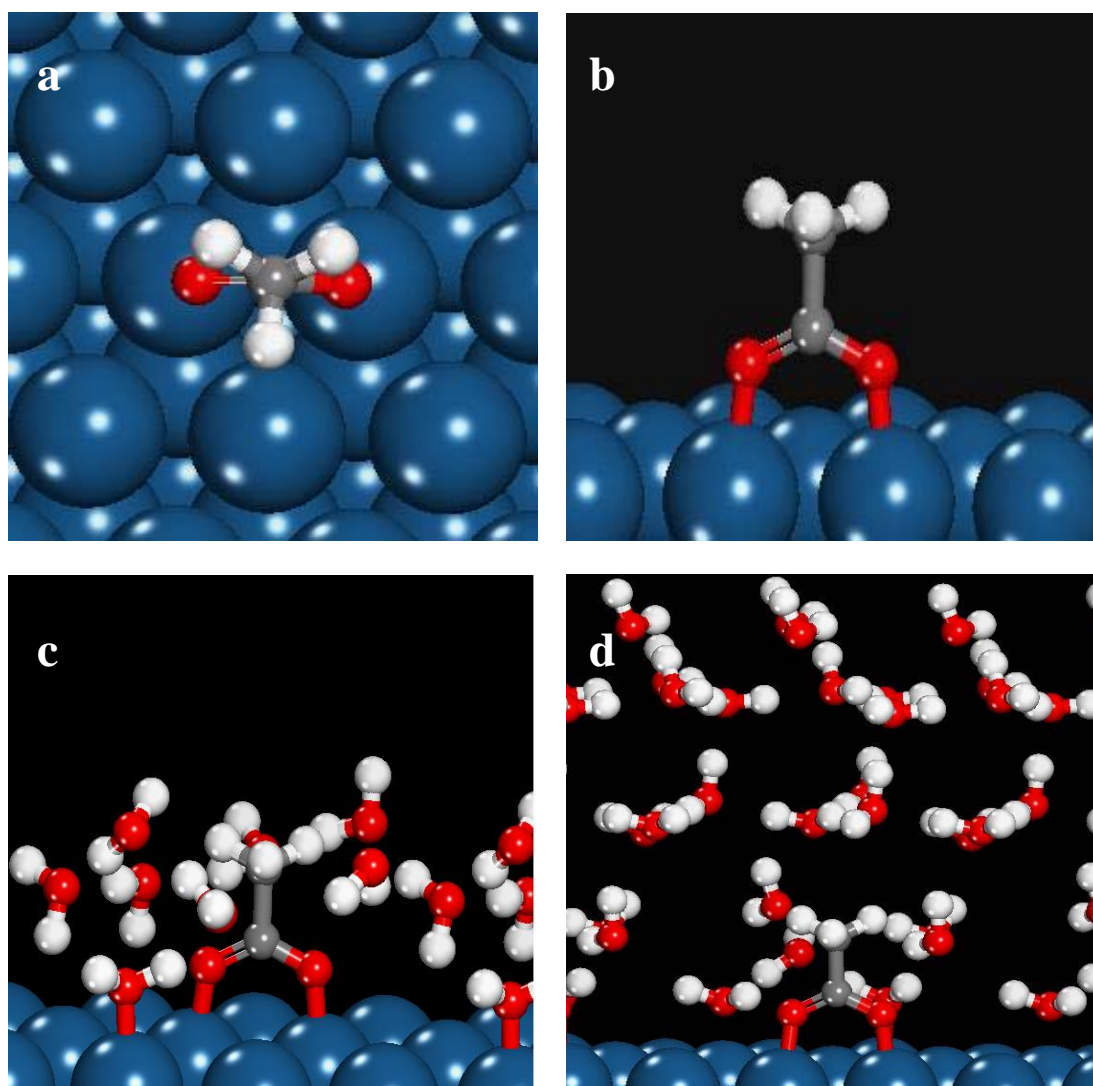


Figure 2-1 Preferred adsorption configuration of acetate over Pt(111) (a) vacuum slab model top view (b) vacuum slab model side view (c) water bilayer-external electric field model (d) double reference method

Effect of surface coverage on acetate adsorption

The adsorption of one acetate molecule to Pt(111) with surface cells of 1×2 , $\sqrt{3} \times \sqrt{3}$, 2×2 , 3×3 , 4×4 was considered using the vacuum slab model. Smaller surface cells represent higher acetate coverage, and adsorption becomes less favorable due to acetate-acetate repulsion at high coverage. Acetate anion forms O-Pt bond at two atop sites, however, because of the methyl group size, adsorption “occupies” three Pt atoms. The adsorption free energy of 1×2 cell is too high, so acetate adsorption on this cell is not possible and it also proves that acetate captures three Pt atoms. Hence, we did not consider this surface cell in our calculations. The 3×3 and 4×4 surface gave the same free energy, therefore we assumed that the free energy of adsorption for higher surface cells equal to the energy of adsorption of acetate on 4×4 surface. Fig. 2-2 shows the adsorption free energy at $U=0$ (SHE) for different surface coverage.

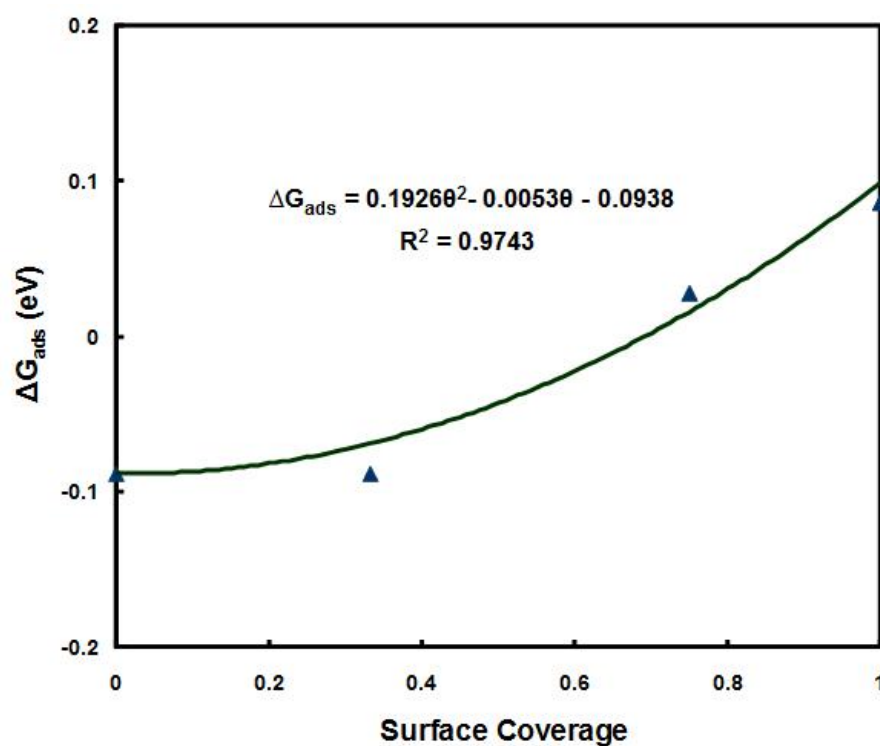


Figure 2-2 Adsorption free energy of acetate to the Pt(111) surface for different surface coverages using the vacuum slab model. (T=298 K, $[\text{CH}_3\text{COO}^-]_{\text{aq}} = 0.2 \text{ M}$, $U=0$ (SHE))

A quadratic function used to fit the data points (eq. 2-19), because it can show better the relation between adsorption free energy and surface coverage than the cubic equation.

$$\Delta G_{ads} = 0.1926\theta^2 - 0.0053\theta + 0.1537 \quad (2-19)$$

The LSV was simulated using the vacuum slab model with the adsorption free energy dependent on coverage (eq. 2-19) and is given in Fig. 2-3. Also given is the same result considering the value of ΔG_{ads} to be coverage independent and constant at the low coverage limit (Fig. 2-3).

The simulated data for acetate adsorption at 30 mV/s and 0.2 M acetate solution is shown in Fig. 2-3.

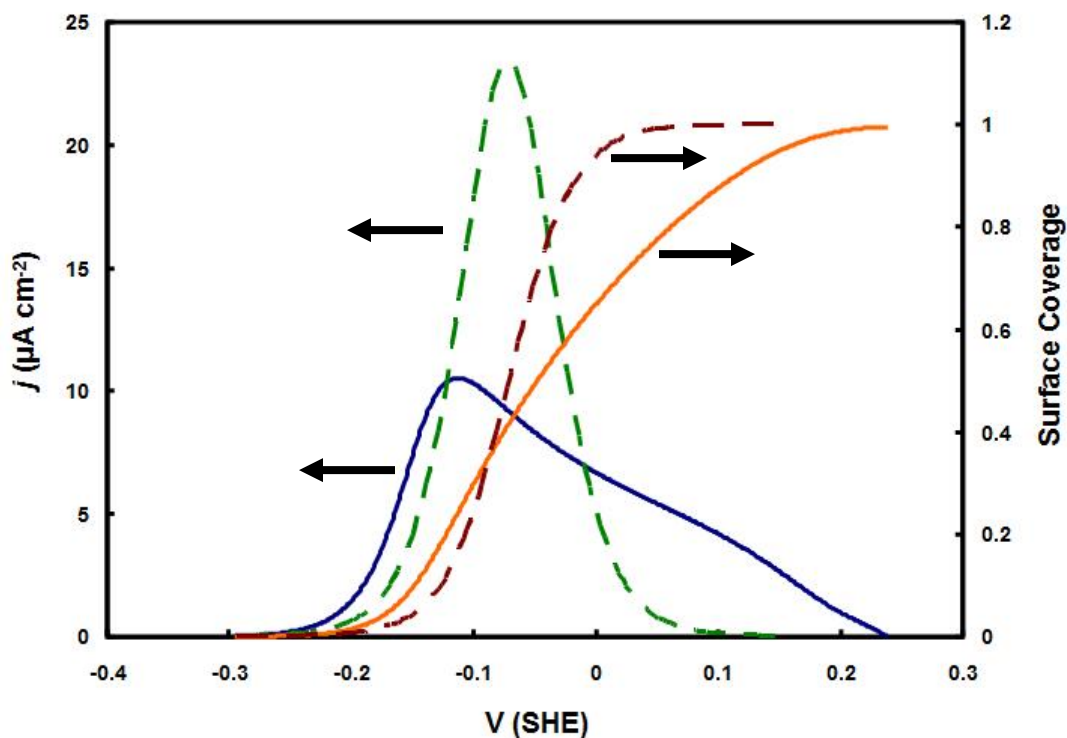


Figure 2-3 Simulated linear sweep voltammetry of acetate adsorption at Pt(111) and the amount of acetate coverage using vacuum slab model with surface coverage effect (solid lines) and without surface coverage effect (dashed lines). ($T=298\text{ K}$, $[\text{CH}_3\text{COO}^-_{\text{aq}}] = 0.2\text{ M}$, $v = 30\text{ mV s}^{-1}$)

We chose these conditions to compare the computational results with the experimental data [25]. The amounts of potential in the all sections are relative to SHE. The adsorption peak begins at -0.28 V and ends near the 0.24 V, and the maximum current of the adsorption peak takes place at -0.12 V. Fukuda and co-workers [25] investigated adsorption of acetate on Pt experimentally and they reported there is a peak related to acetate adsorption which begins near -0.46 V and has 0.35 V width for the same conditions mentioned above. The current and the potential of the maximum point of the peak are tabulated for various methods in Table 2-1.

Comparison between the computational and the experimental work shows that shape of the adsorption peak is consistent with the experimental result except at high surface coverage. As the computational peak is wider than the experimental peak, the difference is unlikely to stem from the neglect of kinetic effects computationally. Kinetic effects would slow the approach to equilibrium and therefore lengthen the experimental tail of the peak rather than provide a narrower peak. The wider peak predicted computationally indicates an over estimation of the repulsion between adsorbates at higher coverages. There are two likely causes for this overestimation. First, the computation required on ordered adsorbate layer matching the unit cell dimensions, while larger super cell structures and disorder is possible experimentally. For the 2x2 cell, for example, computationally we align acetate O atoms on a four of Pt atoms. Secondly, the PW91-DFT approach is known to misrepresent attractive, non-bonded Van der Waals interactions and therefore will overestimate the methyl-methyl repulsion. We therefore conclude that our representation of coverage effect is unsuccessful and the symmetric experimental peak likely indicates a much lesser effect of coverage on adsorption energy.

In another approach we analyze the specific adsorption process by a Langmuir adsorption isotherm with adsorption free energy independent of coverage. The 3x3 surface was employed to calculate the adsorption free energy. Results of this assumption (Fig. 2-3) show good agreement in peak shape and width with experimental data, with a symmetric peak of 0.35 V width. We

conclude that the Langmuir isotherm can predict the adsorption well and we do not consider the coverage effects in further calculations. Vacuum slab model (Langmuir isotherm) predicts that acetate starts adsorbing at -0.25 V, but experimental data shows that adsorption of acetate begins at -0.46 V. There is 0.21 V difference between experimental and computational results. The anion adsorbs in a potential range which $\Delta G_{ads} \leq 0$ in that range. Each computational model gives different free energy of adsorption as a function of potential, so the potential which acetate starts adsorbing depends on the method we use, and inconsistency of that shows the computational model (vacuum slab) was used is not an appropriate model to represent the electrochemical environment for acetate adsorption. Hence, the inconsistency between the starting adsorption potentials predicted by experimental and computational is related to the model we used. So in the next session different computational methods are compared with each other to figure out the results of which model is closer to the experimental data.

Comparison of computational methods for acetate adsorption

Each method applied different approach to model electrode-electrolyte interface, so various amount of adsorption energy calculated. Fig. 2-4 demonstrates the free energy of adsorption as a function of surface potential for each method. The result for vacuum slab is close to applied external electric field rather than to double reference method or water bilayer, because in these two methods only the effect of water displacement is considered and interfacial solvation effect on adsorbate is neglected, so the difference is caused by this effect. Moreover, double reference method and water displacement predict close adsorption energy because of considering both effects on adsorbed molecule in these two methods.

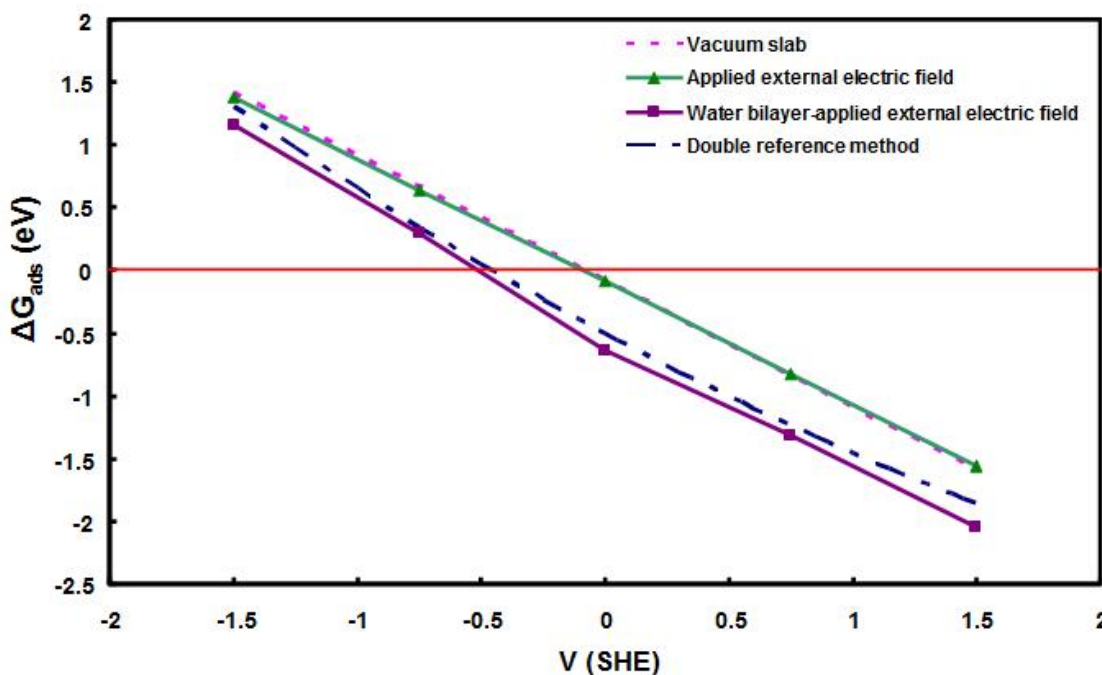


Figure 2-4 Adsorption free energy of acetate on Pt(111) at different potential for different models. (T=298 K, $[\text{CH}_3\text{COO}^-_{\text{aq}}] = 0.2 \text{ M}$)

Hence, the simulated adsorption peaks (Fig. 2-5) for the first two methods are close. The potential which adsorption energy becomes zero, the current and the potential of the maximum point of the peak, starting point of the peak and peak width for each method is tabulated in Table 1. Among the computational methods, double reference method has the lowest difference with the experimental data. Acetate adsorption starting potential predicted by double reference method has 0.14 V difference with experimental data, and there is no difference between peak widths. The current of the maximum point of the adsorption peak (double reference method) is close to the amount Fukuda et al. reported in their work, and also this shows that the assumption of each acetate molecule occupies three Pt atoms is correct. The simulated LSV of double reference method matches better with the experimental results, so we chose the double reference method for further.

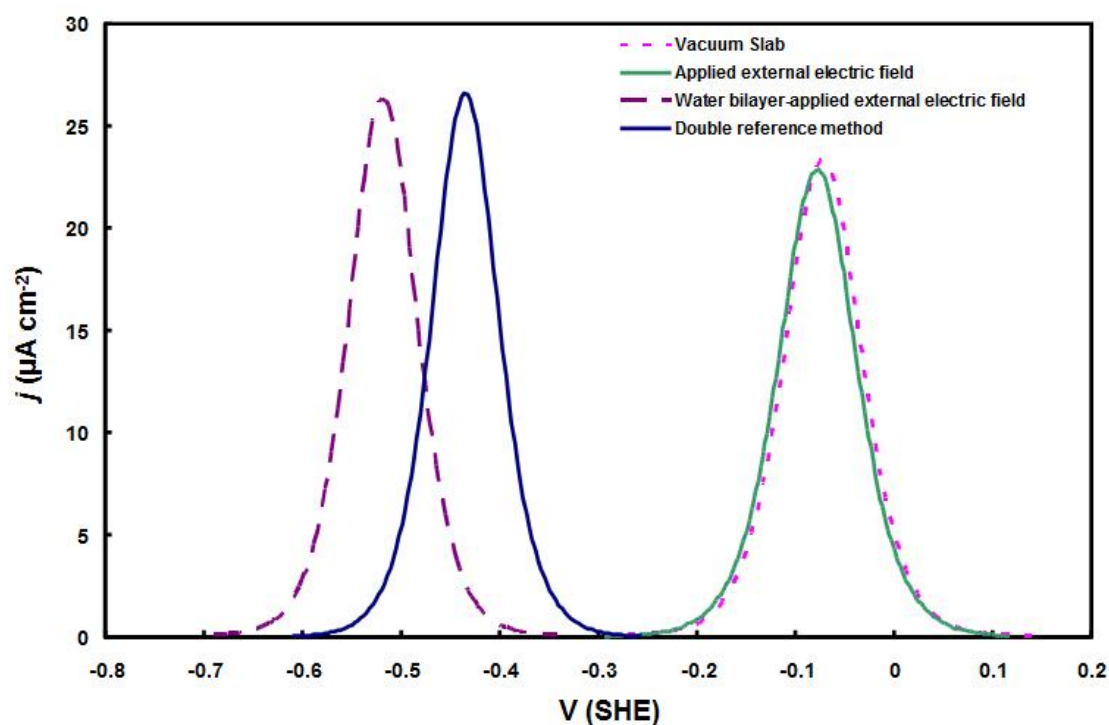


Figure 2-5 Simulated linear sweep voltammetry of acetate adsorption at Pt(111) for different models. ($T=298\text{ K}$, $[\text{CH}_3\text{COO}^-_{\text{aq}}] = 0.2\text{ M}$, $v = 30\text{ mV s}^{-1}$).

Table 2-1 Features of the adsorption peak and free energy of adsorption predicted by different methods

Methods	ΔG_{ads} (eV) at $V=0$ (NHE)	Potential of $\Delta G_{\text{ads}}=0$ (V NHE)	Ads. peak width (V)	Ads. peak starting point (V NHE)	Potential of ads. peak max. point (V NHE)	Current of ads. peak max. point (μAcm^{-2})
Vacuum slab	-0.0885	-0.0885	0.4	-0.25	-0.08	23
Applied external electric field	-0.0885	-0.0885	0.4	-0.25	-0.08	22.5
Water displacement	-0.637	-0.527	0.35	-0.7	-0.51	26
Double reference method	-0.492	-0.449	0.35	-0.6	-0.43	26.5
Experimental results	—	—	0.35	-0.46	-0.36	25

The concentration of acetate we used to simulate the LSV data is different by the acetate concentration in MFCs and MECs, so by an easy recalculation we simulate the LSV data for 0.01 M of acetate (Fig. 2-6). The computational result shows that acetate adsorbs at Pt(111) in lower potential in comparison with the potential that ORR occurs (0.8 V SHE). Hence, adsorption of this anion can block the active sites and reduce the ORR rate. However, this anion adsorbs on platinum surface in higher potential in comparison with the potential that HER happens (-0.45 V SHE), so it has no effect on the HER rate.

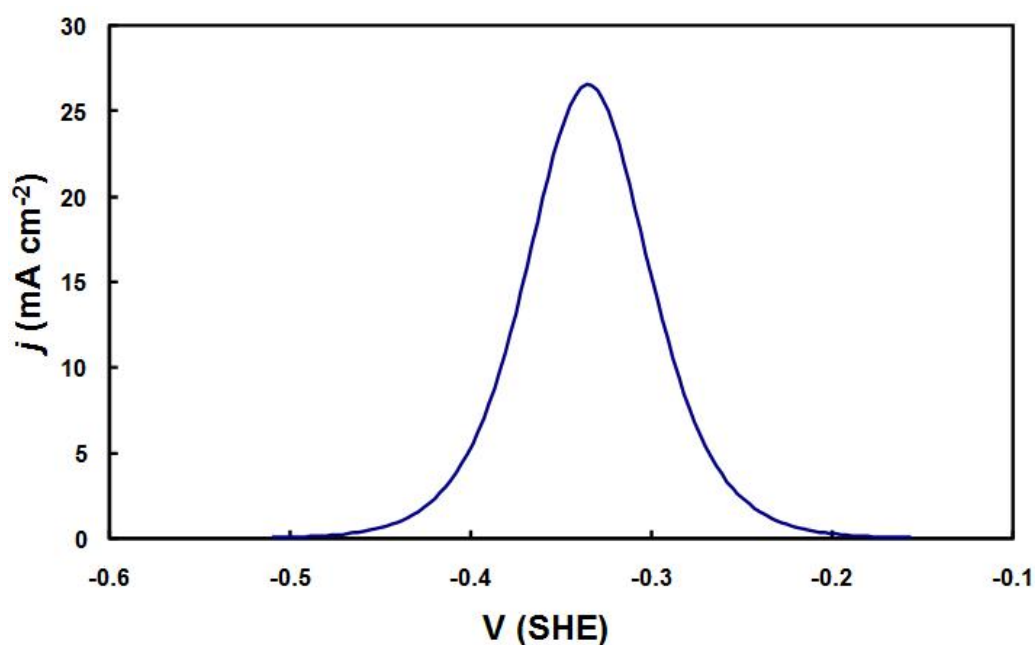
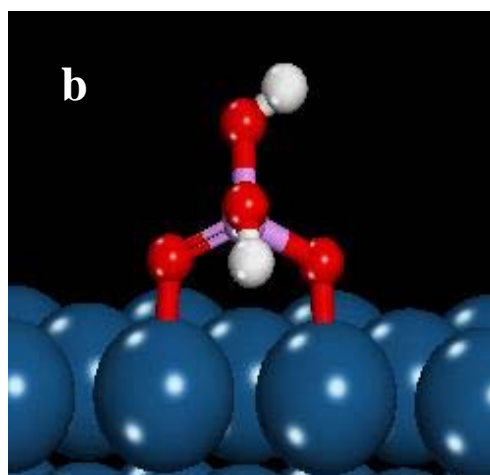
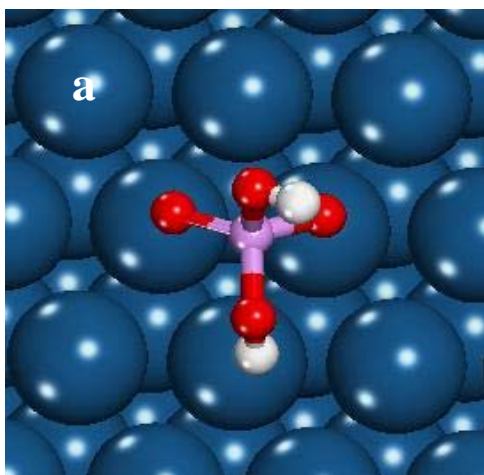


Figure 2-6 Simulated linear sweep voltammetry of acetate adsorption at Pt(111) using double reference method. ($T=298\text{ K}$, $[\text{CH}_3\text{COO}^-_{\text{aq}}] = 0.01\text{ M}$, $v = 30\text{ mV s}^{-1}$)

Dihydrogen phosphate adsorption

Mostany and co-workers [20] reported cyclic voltammogram (CV) at the Pt(111) electrode in NaH_2PO_4 solutions with different concentration. 0.1 M HClO_4 was also included in each solution. They observed the phosphate adsorption peak to shift to lower potential with

increasing concentration of NaH_2PO_4 . In 0.01 M NaH_2PO_4 , the adsorption peak started at 0.35 V (SHE) and ended at 0.6 V (SHE). The adsorption peak is almost symmetric, which may indicate the Langmuir isotherm is a good model to predict the behavior of phosphate adsorption. Bidoia also supposed the Langmuir isotherm as an appropriate model for dihydrogen phosphate adsorption on the platinum surface [23]. Hence, we did not consider the surface coverage effect on adsorption of the phosphate species. In the previous section we showed that by using the double reference method, we are able to predict the anion adsorption peak, so we use this model to simulate the H_2PO_4^- adsorption peak. We also simulate the adsorption peak using the vacuum slab model to show the effect of interfacial solvation on the results. The vacuum slab model with a 3x3 surface cell was applied to obtain the preferred geometry for phosphate species. The 3x3 surface was also used for all of the calculations in this and the next section, because the interactions between adsorbates in this situation are negligible. The preferred geometry of adsorbed dihydrogen phosphate at Pt(111) is shown in Figs. 2-7a, b. Two O atoms and one H atom sit above atop sites. This configuration was maintained in the double reference method (Fig. 2-7c). Each adsorbate molecule therefore occupies three Pt atoms.



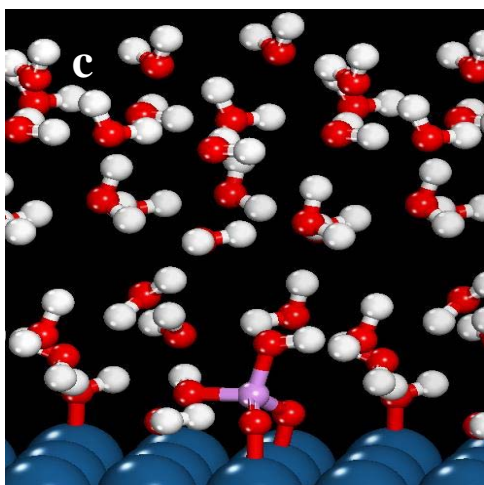


Figure 2-7 Preferred adsorption configuration of dihydrogen phosphate over Pt(111) (a) vacuum slab model top view (b) vacuum slab model side view (c) double reference method.

The adsorption free energy of dihydrogen phosphate over Pt(111) as a function of electrode potential is illustrated in Fig. 2-8.

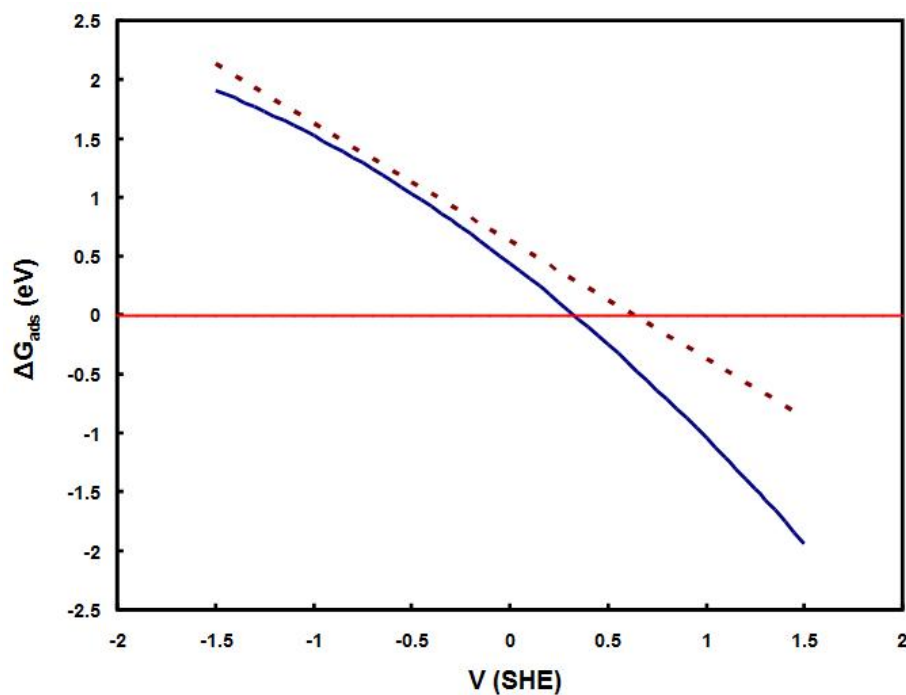


Figure 2-8 Adsorption free energy of dihydrogen phosphate on Pt(111) at different potential for vacuum slab model (dashed line) and the double reference method (solid line). ($T=298\text{ K}$, $[\text{H}_2\text{PO}_4^-]_{\text{aq}} = 0.01\text{ M}$)

The difference between the two models is caused by solvation effects. At high potential, adsorbed H_2PO_4^- has more interaction with water molecules (solvation effect is larger), because it is more polarized, so the difference between two models is bigger in higher potential than lower potential. Fig. 2-9 demonstrates the simulated adsorption peaks of dihydrogen phosphate at platinum for the two different models.

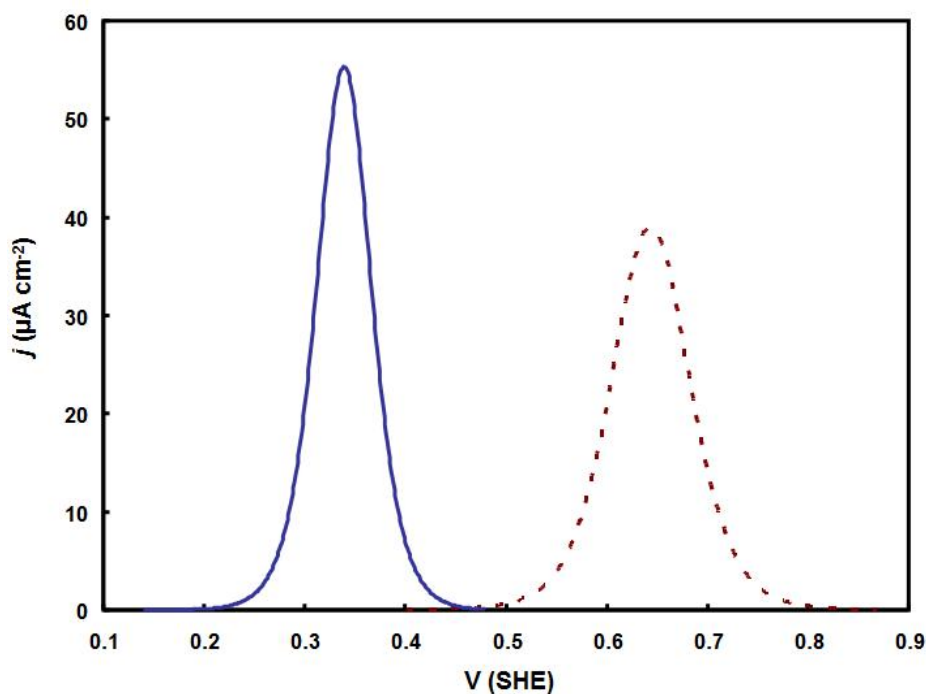
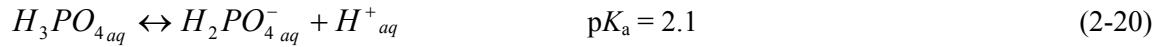


Figure 2-9 Simulated linear sweep voltammetry of dihydrogen phosphate adsorption at Pt(111) for vacuum slab model (dashed line) and the double reference method (solid line). ($T=298\text{ K}$, $[\text{H}_2\text{PO}_4^-]_{\text{aq}} = 0.001\text{ M}$, $v = 50\text{ mV s}^{-1}$)

The concentration of 0.001 M was picked for the simulation, because we want to compare the simulated LSV with experimental results related to $0.1\text{ M HClO}_4 + 0.01\text{ M NaH}_2\text{PO}_4$ solution. According to the following equations, the concentration of H_2PO_4^- in that solution is 0.001 M :



$$\frac{[H^+][H_2PO_4^-]}{[H_3PO_4]} = 10^{-2.1} \quad (2-21)$$

The adsorption peak that was predicted by double reference method starts at 0.35 V (SHE) and ends at 0.6 V (SHE) which is in excellent agreement with experimental data reported by Mostany et al [20], and it substantiates the conclusion that the CV peak in this range is due to $H_2PO_4^-$ adsorption on platinum surface.

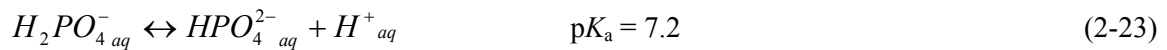
The computational result shows dihydrogen phosphate adsorbs on platinum surface in higher potential in comparison with the potential that HER happens (-0.45 V SHE), so it has no effect on the HER rate. However, this anion adsorbs on Pt(111) in lower potential in comparison with the potential that ORR occurs (0.8 V SHE). Hence, adsorption of this anion can block the active sites and reduce the ORR rate.

Hydrogen phosphate adsorption

Adsorption of hydrogen phosphate can be done through two different processes. This anion can adsorb on platinum electrode from solution directly:



Hydrogen phosphate can also convert to dihydrogen phosphate according to the below equilibrium reaction:



Adsorbed dihydrogen phosphate can convert to adsorbed hydrogen phosphate:





We first consider hydrogen phosphate adsorption to the Pt(111) surface from solution (eq. 2-22) and later we investigate the other process. Like the other two anions, we need to find the orientation of adsorbed HPO_4^{2-} with the lowest free energy. This anion adsorbs on Pt(111) with three hydrogen-less oxygen atoms on three atop sites (Figs 2-10a, b), so the coverage over the 3x3 surface is 1/3 ML. Fig. 2-10c shows that in double reference method, the preferred orientation did not change.

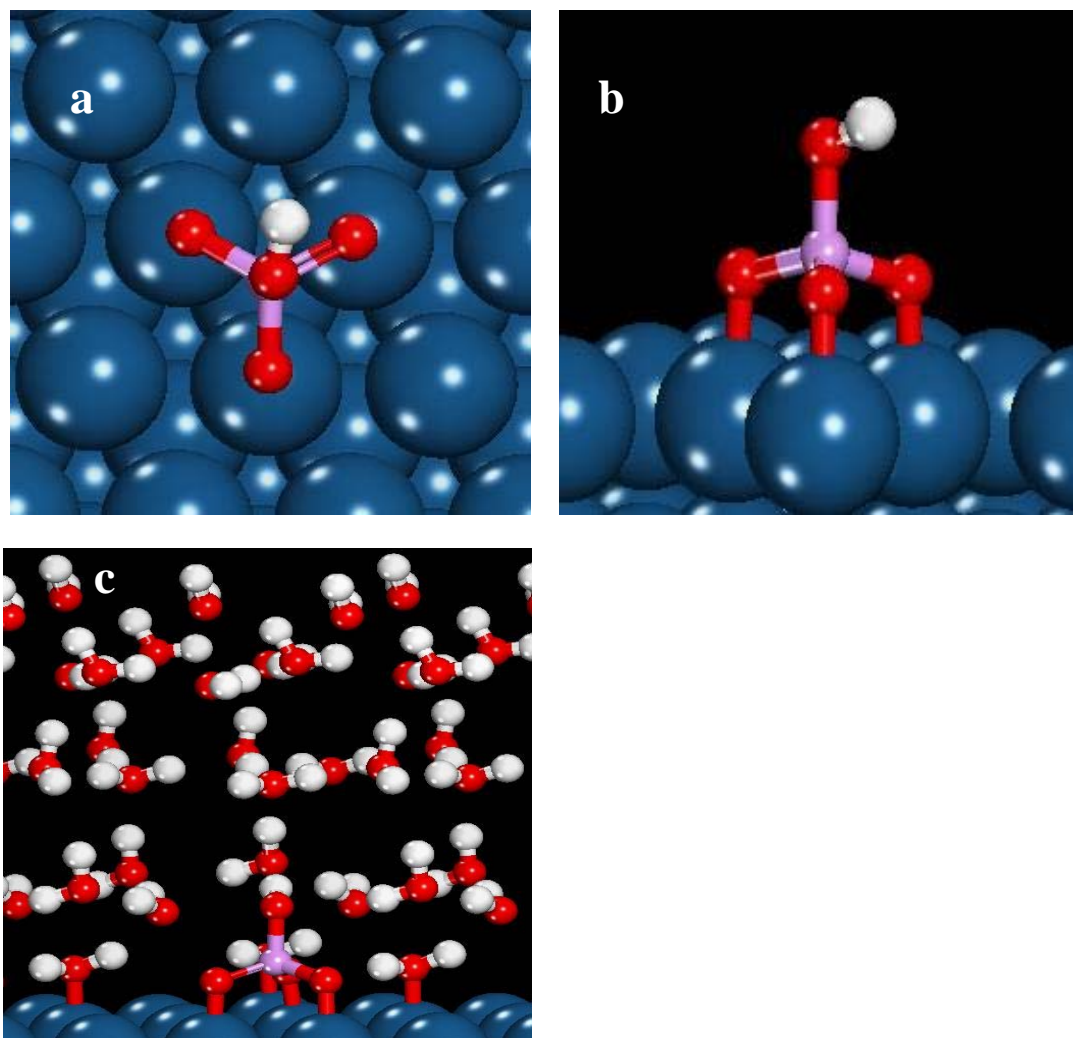


Figure 2-10 Preferred adsorption configuration of hydrogen phosphate over Pt(111) (a) vacuum slab model top view (b) vacuum slab model side view (c) double reference method

The adsorption energy as a function of electrode potential for the double reference method and vacuum slab is demonstrated in Fig. 2-11. The slope of the curves is sharper compare with curves for acetate (Fig. 2-4) and dihydrogen phosphate (Fig. 2-8) because during the adsorption of hydrogen phosphate two electrons transferred to the metal. The Langmuir isotherm is assumed to rule the adsorption process.

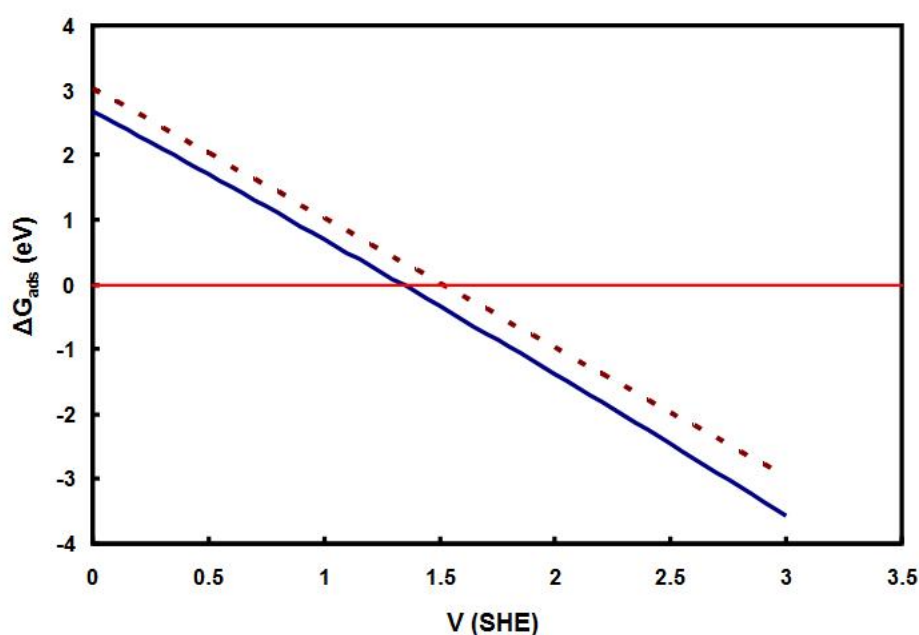


Figure 2-11 Adsorption free energy of hydrogen phosphate on Pt(111) at different potential for vacuum slab model (dashed line) and the double reference method (solid line). (T=298 K, $[\text{HPO}_4^-]_{\text{aq}} = 0.01 \text{ M}$)

The results of simulated LSV are shown in Fig. 2-12, and like the other two anions, there is a difference between vacuum slab model and double reference method caused by solvation effects. Adsorption of HPO_4^{2-} can also be done through equations 2-23 to 2-25. The equation 2-23 is in equilibrium so the free Gibbs energy difference of this reaction is zero. We calculated the adsorption free energy of H_2PO_4^- (equation 2-24) in last section, so all we need to know is the

free Gibbs energy difference of reaction 2-25. First we have to find out $G_{H_{aq}^+}$ which we can calculate by using the following equation:

$$G_{H_{aq}^+} = G_{H_2PO_4^{2-}} - G_{HPO_4^{2-}} \quad (2-25)$$

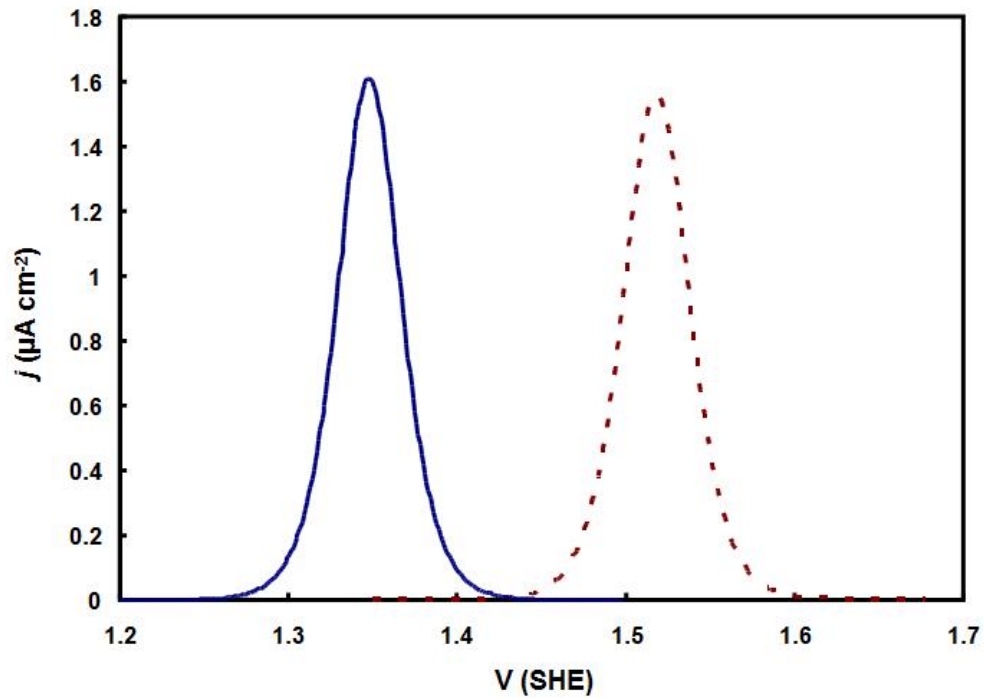


Figure 2-12 Simulated linear sweep voltammetry of hydrogen phosphate adsorption at Pt(111) for vacuum slab model (dashed line) and the double reference method (solid line). (T=298 K, $[H_2PO_4^-] = 0.01$ M, $v = 1$ mV s⁻¹)

If we assume that we solved 0.01 M HPO_4^{2-} in water and the initial pH was 7, we are able to calculate the concentration of $H_2PO_4^-$, HPO_4^{2-} , H^+ in solution by equation 2-23. After calculating the concentration we are able to find the $G_{H_{aq}^+}$ and by having this parameter we can calculate the free Gibbs energy difference of reaction 2-25 and 2-26. The sum of ΔG of these

two reactions at zero surface potential same as the ΔG of reaction 2-22, so these reactions happen at the same potential.

From the computational results we can understand that hydrogen phosphate cannot change the ORR and HER because it adsorbs on platinum electrode in higher potential in comparison with the potentials that these two reactions occur (-0.45 V SHE and 0.8 V SHE).

Chapter 3

LSV of oxygen reduction and hydrogen evolution reaction on platinum surface in presence of anions

In this chapter, linear sweep voltammetry (LSV) is used to evaluate HER and ORR kinetics in the presence of anions. The presence of acetate and dihydrogen phosphate slowed the rate of ORR. The rate of HER was increased in the presence of dihydrogen phosphate which is caused by the weak acid effect of this anion. The inclusion of acetate or hydrogen phosphate to the solution did not change the HER kinetics.

Experimental methods

The experimental setup consisted of an electrochemical cell (AFCELL1 standard voltammetry cell, Pine research instrumentation) which contained a 200 ml electrolyte solution, 5 mm platinum disk working electrode (AFE3T050PT platinum RDE tip, Pine research instrumentation), platinum wire as the counter electrode, and a Ag/AgCl reference electrode (Fig. 3.1). Before each experiment, the working electrode was polished in two steps: first with 1 μm alumina (rough polishing) and second with 0.05 μm alumina (soft polishing). For the oxygen reduction reaction experiments, each solution was aerated for 30 minutes before starting the experiment. The hydrogen evolution and oxygen reduction reaction were recorded with 5 mVs^{-1} scan rate, initiating at potentials greater than the reaction equilibrium potential and scanning in the negative direction, using the potentiostat (PC4/750TM, Gamry, Warminster). All of the chemicals were bought from Sigma-Aldrich Company. All of the experiments were performed at 30 °C.

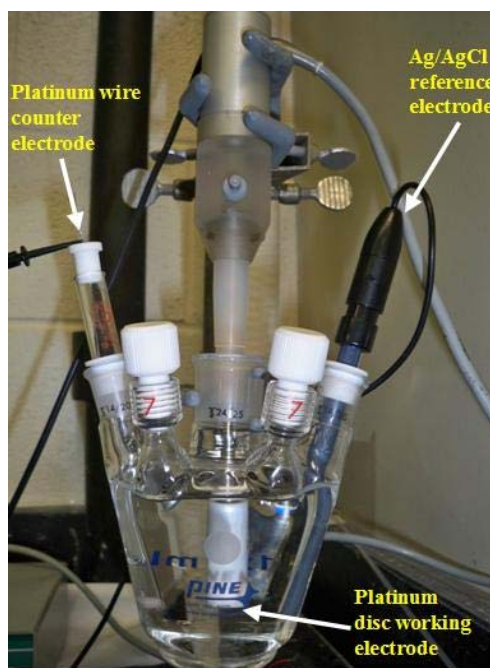


Figure 3-1 Experimental setup to record the LSV data

LSV of the oxygen reduction reaction

In the previous chapter, it was shown that acetate and dihydrogen phosphate with concentration of 0.01 M adsorb at potentials greater than -0.5 V (SHE) and 0.2 V (SHE) respectively. The equilibrium potential of ORR is 0.8 V (SHE), and comparing this potential with the potential that acetate and dihydrogen phosphate start adsorbing shows that these anions can adsorb and possibly block active sites of the cathode surface during ORR. Hence, adsorption of these anions may reduce the ORR rate. Hydrogen phosphate adsorbs on the platinum surface (1.2 V SHE) after the ORR occurs, so it cannot affect the rate of the reaction. Fig. 3-2 demonstrates the LSV data for ORR. Perchloric acid was chosen as the reference because ClO_4^- is a non-adsorbing anion, so this anion has no effect on the rate of ORR. By adding sodium acetate and

sodium dihydrogen phosphate the ORR rate decreased, as expected. The computational results corroborate that this decrease is caused by the adsorption of anion on the platinum surface.

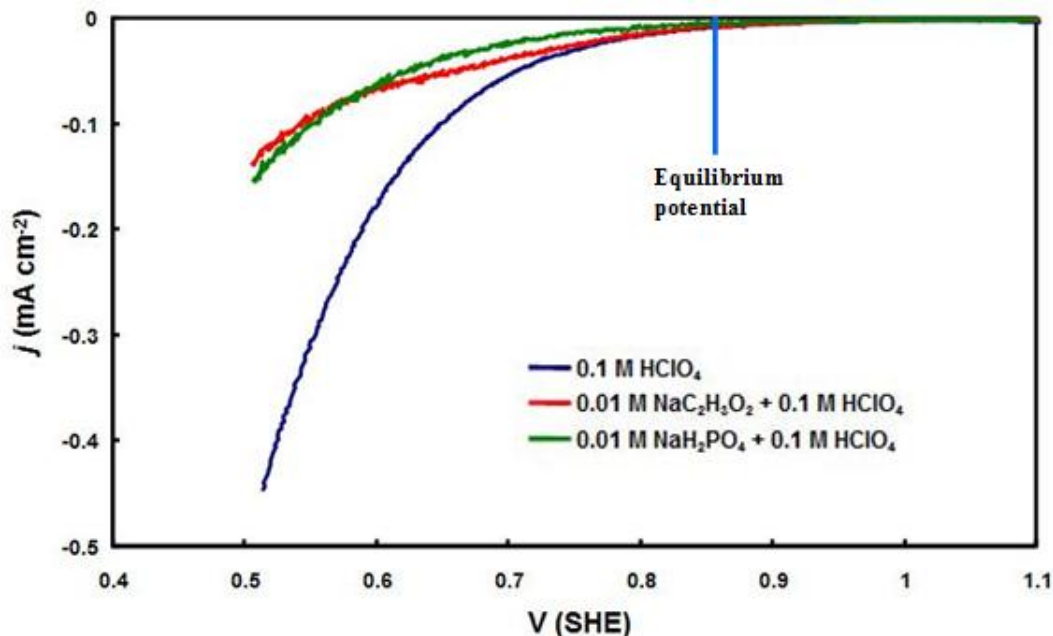


Figure 3-2 Linear sweep Voltammograms for ORR at the platinum disc. All LSV recorded at $v = 5 \text{ mVs}^{-1}$

LSV of the hydrogen evolution reaction

As shown in chapter 2, all of the anions including acetate and phosphate species adsorbed at platinum surface at potentials above the equilibrium potential of HER (-0.42 V SHE). Therefore, these anions will not reduce the active sites of cathode. The experimental results (Fig. 3-3) show that the HER rate is increased in the presence of H_2PO_4^- anions. There are two possible theories for this phenomenon. “Electrochemical deprotonation” first adsorbs H_2PO_4^- to the surface, which is then reduced (deprotonated). Our calculations showed at the potential that HER occurs, the adsorbed coverage of this anion is effectively zero. Hence, the weak acid effect is better explained by solution phase deprotonation of H_2PO_4^- recreating proton depleted from the solution.

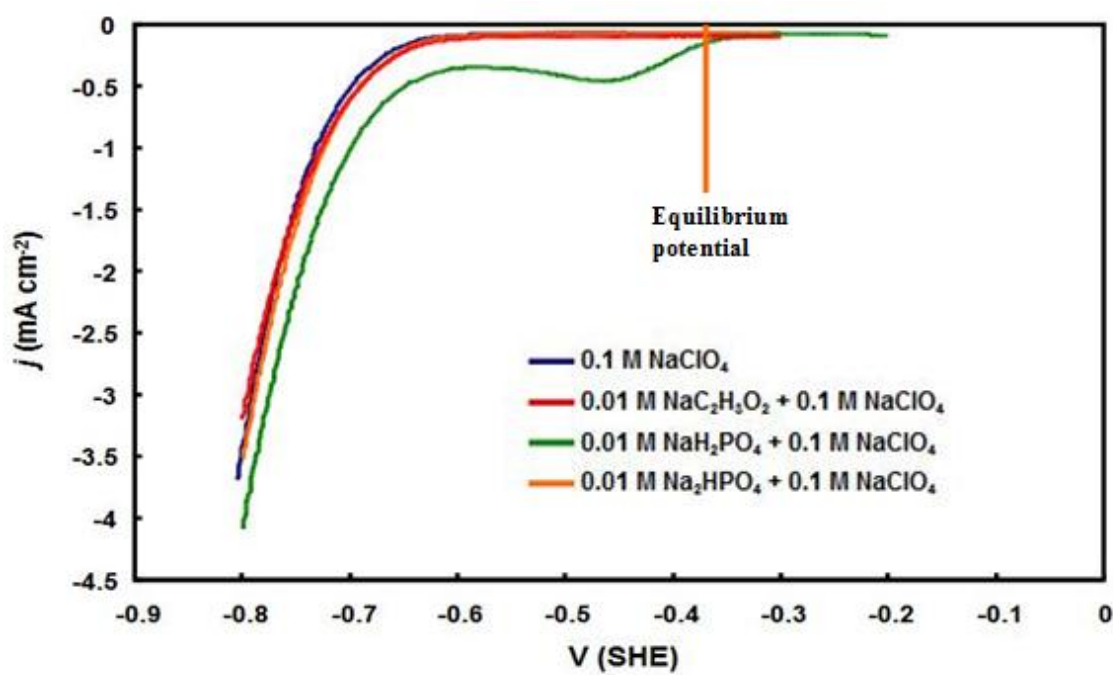


Figure 3-3 Linear sweep Voltammograms for HER at the platinum disc. All LSV recorded at $v = 5 \text{ mVs}^{-1}$

Chapter 4

Conclusions

The effects of anions on cathodic reactions in MFCs and MECs were examined by using computation (DFT methods) and experiment (LSV). Among the four different models used to simulate the adsorption of anions (acetate, dihydrogen and hydrogen phosphate) at Pt(111), we found the double reference method is the best model simulate the anion adsorption on platinum surface, because the LSV predicted by this model is more consistent than other models. Experimental results show that surface coverage has little effect on anion adsorption and Langmuir isotherm is a good model to predict the adsorption process, so we neglected the surface coverage effect in our LSV simulation.

The computational results showed that acetate and dihydrogen phosphate adsorb at Pt(111) in lower potentials in comparison with the potential that ORR occurs. Hence, adsorption of these anions can block the active sites and reduce the ORR rate. However, these anions adsorb on platinum surface in higher potentials in comparison with the potential that HER happens, so they have no effect on the HER rate. Hydrogen phosphate cannot change the ORR and HER because it adsorbs on platinum electrode in higher potentials in comparison with the potentials that these two reactions occur.

Experimental LSV studies were used to evaluate HER and ORR kinetics in the presence of various anions. Experimental results showed that the presence of acetate and dihydrogen phosphate reduced the ORR rate, which is consistent with the computational results indicating the Pt surface is blocked by adsorbed anions under these conditions. The presence of anions had no effect on HER except dihydrogen phosphate which increased the HER rate due to the weak acid effect of this anion.

References

- [1] B.E. Logan, B. Hamelers, R. Rozendal, U. Schröder, J.r. Keller, S. Freguia, P. Aelterman, W. Verstraete, K. Rabaey, 40 (2006) 5181-5192.
- [2] B.E. Logan, D. Call, S. Cheng, H.V.M. Hamelers, T.H.J.A. Sleutels, A.W. Jeremiasse, R.A. Rozendal, 42 (2008) 8630-8640.
- [3] M.D. Merrill, B.E. Logan, 191 (2009) 203-208.
- [4] D. Call, B.E. Logan, 42 (2008) 3401-3406.
- [5] Damjanov.A, V. Brusic, *Electrochim. Acta* 12 (1967) 615-&.
- [6] T.J. Schmidt, U.A. Paulus, H.A. Gasteiger, R.J. Behm, 508 (2001) 41-47.
- [7] N.M. Markovic, H.A. Gasteiger, B.N. Grgur, P.N. Ross, 467 (1999) 157-163.
- [8] G. Horányi, 2 (1998) 237-241.
- [9] S. Da Silva, R. Basséguy, A. Bergel, 49 (2004) 4553-4561.
- [10] P. O'Neill, F. Busi, V. Concialini, O. Tubertini, 284 (1990) 59-65.
- [11] K. Takehara, Y. Ide, T. Nakazato, N. Yoza, 293 (1990) 285-290.
- [12] Z. Du, H. Li, T. Gu, 25 464-482.
- [13] G.-C. Gil, I.-S. Chang, B.H. Kim, M. Kim, J.-K. Jang, H.S. Park, H.J. Kim, 18 (2003) 327-334.
- [14] A.W. Jeremiasse, H.V.M. Hamelers, J.M. Kleijn, C.J.N. Buisman, 43 (2009) 6882-6887.
- [15] S.C.S. Lai, M.T.M. Koper, *Faraday Discuss.* 140 (2008) 399-416.
- [16] M.A. Climent, M.J. Valls, J.M. Feliu, A. Aldaz, J. Clavilier, *J. Electroanal. Chem.* 326 (1992) 113-127.
- [17] J.M. Feliu, M.J. Valls, A. Aldaz, M.A. Climent, J. Clavilier, *J. Electroanal. Chem.* 345 (1993) 475-481.
- [18] S. Taguchi, A. Aramata, *J. Electroanal. Chem.* 457 (1998) 73-81.
- [19] T. Fukuda, A. Aramata, *J. Electroanal. Chem.* 440 (1997) 153-161.
- [20] J. Mostany, P. Martinez, V. Climent, E. Herrero, J.M. Feliu, *Electrochim. Acta* 54 (2009) 5836-5843.
- [21] M.A. Habib, J.O. Bockris, *J. Electrochem. Soc.* 132 (1985) 108-114.
- [22] S. Ye, H. Kita, A. Aramata, *J. Electroanal. Chem.* 333 (1992) 299-312.
- [23] E.D. Bidoia, 408 (2005) 1-4.
- [24] J.M. Orts, R. Gomez, J.M. Feliu, A. Aldaz, J. Clavilier, *Electrochim. Acta* 39 (1994) 1519-1524.
- [25] T. Fukuda, A. Aramata, *J. Electroanal. Chem.* 467 (1999) 112-120.
- [26] A. Rodes, E. Pastor, T. Iwasita, *J. Electroanal. Chem.* 376 (1994) 109-118.
- [27] R. Lenk, M. Bonzon, H. Greppin, *Chem. Phys. Lett.* 76 (1980) 175-177.
- [28] O. Teschke, G. Ceotto, E.F. de Souza, *Phys. Rev. E* 64 (2001) 10.
- [29] A. Glebov, A.P. Graham, A. Menzel, J.P. Toennies, *J. Chem. Phys.* 106 (1997) 9382-9385.
- [30] M. Ito, *Surf. Sci. Rep.* 63 (2008) 329-389.
- [31] A. Panchenko, M.T.M. Koper, T.E. Shubina, S.J. Mitchell, E. Roduner, *J. Electrochem. Soc.* 151 (2004) A2016-A2027.
- [32] M.P. Hyman, J.W. Medlin, 109 (2005) 6304-6310.
- [33] J. Rossmeisl, E. Skulason, M.E. Bjorketun, V. Tripkovic, J.K. Nørskov, *Chem. Phys. Lett.* 466 (2008) 68-71.
- [34] E. Skulason, G.S. Karlberg, J. Rossmeisl, T. Bligaard, J. Greeley, H. Jonsson, J.K. Nørskov, *Phys. Chem. Chem. Phys.* 9 (2007) 3241-3250.
- [35] R. Jinnouchi, A.B. Anderson, *Phys. Rev. B* 77 (2008) 18.

- [36] J.K. Norskov, J. Rossmeisl, A. Logadottir, L. Lindqvist, J.R. Kitchin, T. Bligaard, H. Jonsson, *J. Phys. Chem. B* 108 (2004) 17886-17892.
- [37] A.B. Anderson, D.B. Kang, *J. Phys. Chem. A* 102 (1998) 5993-5996.
- [38] C.D. Taylor, S.A. Wasileski, J.S. Filhol, M. Neurock, *Phys. Rev. B* 73 (2006) 16.
- [39] J.S. Filhol, M. Neurock, *Angew. Chem.-Int. Edit.* 45 (2006) 402-406.
- [40] S.U.M. Khan, G.J. Liu, *J. Electroanal. Chem.* 270 (1989) 237-252.
- [41] P. Oneill, F. Busi, V. Concialini, O. Tubertini, *J. Electroanal. Chem.* 284 (1990) 59-65.
- [42] S. Daniele, M.A. Baldo, F. Simonetto, *Anal. Chim. Acta* 331 (1996) 117-123.
- [43] G. Kresse, J. Hafner, 47 (1993) 558.
- [44] G. Kresse, J. Furthmüller, 54 (1996) 11169.
- [45] G. Kresse, J. Furthmüller, 6 (1996) 15-50.
- [46] J.P. Perdew, J.A. Chevary, S.H. Vosko, K.A. Jackson, M.R. Pederson, D.J. Singh, C. Fiolhais, 46 (1992) 6671.
- [47] G. Kresse, D. Joubert, 59 (1999) 1758.
- [48] G. Rostamikia, M.J. Janik, *J. Electrochem. Soc.* 156 (2009) B86-B92.
- [49] S. Cabani, P. Gianni, V. Mollica, L. Lepori, *J. Solut. Chem.* 10 (1981) 563-595.
- [50] P. George, R.J. Witonsky, M. Trachtman, C. Wu, W. Dorwart, L. Richman, W. Richman, F. Shurayh, B. Lentz, 223 (1970) 1-15.
- [51] M. Morgenstern, J. Muller, T. Michely, G. Comsa, *Z. Phys. Chemie-Int. J. Res. Phys. Chem. Chem. Phys.* 198 (1997) 43-72.